02

Effect of yttrium content on luminescent properties and charge localization in $(0.23ZrO_2-0.77HfO_2)-Y_2O_3-Eu_2O_3$ ceramics

© E.V. Dementeva, G.A. Gusev, P.A. Dementev, K.N. Orekhova, M.V. Zamoryanskaya

Ioffe Institute,
St. Petersburg, Russia

e-mail: dementeva@mail.ioffe.ru

Received October 29, 2025
Revised October 29, 2025
Accepted December 05, 2025

The main objective of the study was to determine the effect of yttrium concentration on charge localization in $(0.23ZrO_2-0.77HfO_2)-Y_2O_3-Eu_2O_3$ ceramics. In this work, $(0.23ZrO_2-0.77HfO_2)-Y_2O_3-Eu_2O_3$ ceramics with different yttrium contents were synthesized by the co-precipitation technique, and its composition and luminescent properties were studied. All samples were stabilized in the cubic phase and exhibited red luminescence with characteristic emission bands of Eu^{3+} ions. It was shown that an increase in the yttrium content leads to an increase in the content of electron traps associated with oxygen vacancies. The obtained results can be used in the development of new thermoluminescent detectors.

Keywords: hafnium dioxide, zirconium dioxide, yttrium oxide, europium, cathodoluminescence, ceramics, thermoluminescent detectors, oxygen vacancies, electron traps.

DOI: 10.61011/EOS.2025.12.63188.8720-25

Introduction

Due to the increasing need for nuclear waste disposal, as well as research on the consequences of environmental disasters, development of radiometric devices with different sensitivity thresholds is an urgent issue. Thermoluminescence dosimeters are widely used for these purposes. Among the essential objectives is developing the radiation-resistant thermoluminescence dosimeters (TLD) capable of measuring high doses of ionizing radiation. One of the promising materials for TLD is yttrium-stabilized zirconia (YSZ) [1,2], however, its transparency for neutrons makes its application scope limited. In contrast to it, hafnium with its five stable isotopes (^{176}Hf, ^{177}Hf, ^{178}Hf, ^{179}Hf, ^{180}Hf) absorbs the neutrons with high efficiency. In this regard, the replacement of zirconium with hafnium in cubic ceramics may be very promising in the development of dosimeters that detect high-energy ionizing radiation fluxes. Despite the fact that hafnium is very close in its chemical properties to zirconium, the technological conditions for the production and properties of hafnium-based materials may differ greatly from zirconium-based materials.

Hafnium dioxide-based materials exhibit high mechanical, chemical, and radiation stability. Under atmospheric pressure the pure HfO_2 has three crystalline modifications: monoclinic (M, stable up to 1923 K) [3], tetragonal (T, 1923–2530 K) and cubic (C, above 2530 K) [4]. The stabilization temperatures of various crystalline modifications of hafnium oxide are significantly higher than the stabilization temperatures for zirconium oxide. Stabilization of the cubic phase at room temperature is achieved by the introduction of 8–20 mol.% trivalent cations (Y^{3+}, Sc^{3+}, etc.), which leads to the formation of solid solutions with a fluorite-type structure.

Hafnium dioxide and ceramics based on cubic stabilized hafnium oxide were studied in terms of thermal stability [2,5–7], scintillation [8] and thermoluminescence properties [9] depending on alloying elements or synthesis conditions. The traps in thin films HfO_2 and $Hf_xZr_{x-1}O_2$ are well studied [10–13], however, these studies didn't cover bulk ceramic samples. The effect of zirconium/hafnium ratio on the basic properties of ceramics was investigated in [14,15]. It has also been shown that if zirconium is substituted with hafnium it leads to the appearance of deep trap levels, which suggests the possibility of using such materials for thermoluminescence dosimetry [16].

To examine the fine structural changes of wide-band materials and the local symmetry of the ions that make up their composition, a luminescent ion can be used with an isomorphic substitution one of the material's elements. The most well-known ion used for such studies is the trivalent europium ion. It has a bright luminescence in the red region of the spectrum, and its spectra are sensitive to the local ion environment [17–19].

The purpose of this study was to synthesize the ceramics $(0.23ZrO_2-0.77HfO_2)-Y_2O_3$-$Eu_2O_3$ with different yttrium content and to investigate the effect of yttrium content on the luminescent properties of ceramics and charge localization.

Sample synthesis and study methods

By method of co-precipitation 4 charges of $(0.23ZrO_2-0.77HfO_2)-Y_2O_3-Eu_2O_3$ were fabricated

with various content of yttrium. Ceramics was synthesized from the resulting series of charges for 3 h at a temperature of 1500°C. Further, individual samples will have a short name like xEu-yYSZH, where x and y — mole content of Eu_2O_3 and content of Y_2O_3 rounded up to whole percentage numbers.

For electron microprobe analysis (EMPA) and cathodoluminescence (CL) studies, the samples were sawn, fixed in epoxy resin, and a carbon film was sprayed onto their surface to ensure electron flow. The elemental composition of the studied samples was obtained by EMPA. The study of the composition was carried out on a CAMEBAX electron probe microanalyzer equipped with four X-ray spectrometers with the following electron beam parameters: electrons energy $U = 20$ keV, absorbed current $I = 15$ nA, beam diameter $d = 2\,\mu$m. For analysis, the analytical line L_α was taken for all the elements. The standards selected included metallic hafnium (for Hf), $Y_3Al_5O_{12}$ compounds (for determination of Y) and $EuPO_4$ (for determination of Eu). The oxygen content was calculated based on stoichiometry. The elemental composition was measured in several (minimum five) randomly selected areas of the samples.

The luminescent properties of the ceramics samples were studied by cathodoluminescence (CL) using the same CAMEBAX setup, additionally equipped with an optical spectrometer. The spectra of CL samples were obtained within the wavelength range of $\lambda = 350-800$ nm: electron beam energy $U = 20$ keV, absorbed current $I = 20$ nA and the beam diameter $d = 5\,\mu$m. The CL images of the samples were obtained under the following conditions: the electron beam energy $U = 20$ keV, absorbed current $I = 100$ nA and beam diameter $d = 200\,\mu$m. Time measurements were carried out with the electron beam diameter of $40\,\mu$, since measurements with a smaller diameter led to a greater spread of the determined parameters [20].

The thermoluminescence method is traditionally used to study the trapped states [16]. Also, to determine the type of traps and their contents, a method based on measuring the dynamics of absorbed current and CL intensity by a scanning electron microscope can be used [13].

The dependences of CL intensity at a wavelength of 500 nm and the absorbed current on the irradiation time during stationary electron beam irradiation were obtained with the following electron beam parameters: $U = 20$ keV, absorbed current of $I = 50$ nA and the beam diameter of $d = 50\,\mu$m.

When the sample is irradiated with an electron beam, nonequilibrium charge carriers are generated. If there are traps in a sample, then from the moment the sample is irradiated with an electron beam, they capture charge carriers (electrons or holes). In general, the dependence of the absorbed current on the time of electron beam irradiation for a sample containing one type of electron and hole traps can be described as follows:

$$J = J_0 - A_e \exp(-t/\tau_e) + A_h \exp(-t/\tau_h),$$

Table 1. Elemental composition of samples according to EPMA data

Name of sample	HfO_2, mol%	ZrO_2, mol%	Y_2O_3, mol%	Eu_2O_3, mol%	Hf/(Hf + Zr)
0.4Eu−9YSZH	72.2	18.6	8.8	0.4	0.79
0.6Eu−11YSZH	68.3	20.5	10.5	0.6	0.77
0.4Eu−14YSZH	66.2	19.5	13.9	0.4	0.77
0.4Eu−16YSZH	64.5	19.3	15.7	0.4	0.77

where the exponent $A_e \exp(t/\tau_e)$ describes the contribution of electronic traps, and the exponent $A_h(-t/\tau_h)$ is the contribution of hole traps. Coefficients $1/\tau_e$ and $1/\tau_h$ — delineate the probability of the electrons and holes capture, respectively, by the traps. The number of traps is found as $A_e\tau_e$. It should be noted that there can be several types of traps for carriers of both signs, and accordingly, experimental dependencies can be significantly more complicated. Thus, measuring the dynamics of the absorbed current under continuous electron beam irradiation makes it possible to investigate the capture of charge carriers by traps.

To examine the structural changes of wide-band materials and the local symmetry of the ions that make up their composition, a luminescent ion can be used with an isomorphic substitution one of the material's elements. The most well-known ion used for such studies is the trivalent europium ion. It has a bright luminescence in the red region of the spectrum, and its spectra are sensitive to the local ion environment [16–18,20]. Transition $^5D_0^7\_F_1$ Eu^{3+} is magnetic dipole (MD) transition, and its intensity weakly depends on the local ion environment $^{3+}$, in contrast to the electric dipole (ED) transition $^5D_0^7\_F_2$. In crystal structures with an inversion center, the intensity of ED transition $^5D_0^7\_F_2$ decreases due to the parity prohibition, and the MD transition in the luminescence spectrum $^5D_0^7\_F_1$ becomes the most intense [20]. The relationship $I_{(ED)}/I_{(MD)}$ is called an asymmetry coefficient, and the bigger it, the lower the symmetry of the local position occupied by Eu^{3+}. Such studies may be carried out based on the local CL method. This makes it possible to combine studies of local symmetry and trap states using a single instrument, a scanning electron microscope.

Results and discussion

Elemental composition and crystalline structure

Elemental composition of samples by EPMA method was determined (Table 1). The obtained values of the elements content corresponded to the planned ones, the deviation did not exceed the measurement error limits for all samples (10% rel. for europium, 2% rel. for other elements in the samples). The homogeneity of the composition was investigated for all samples of the series, and it was

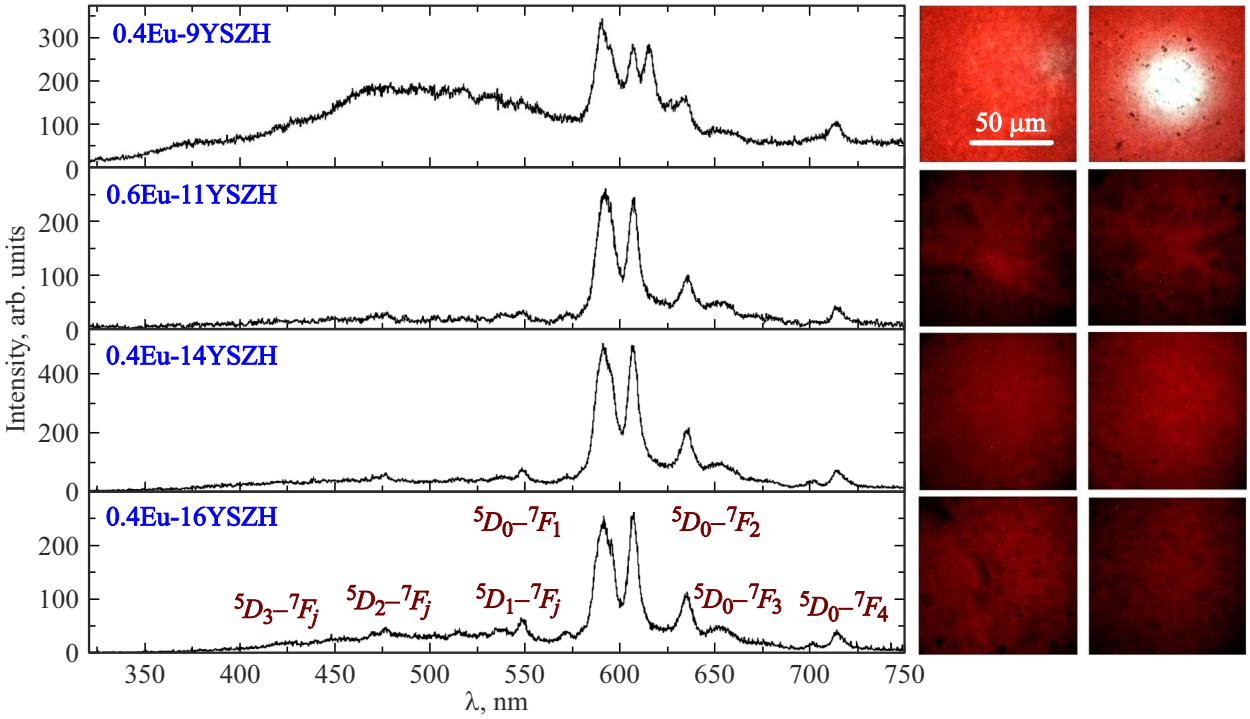

Figure 1. Spectra and CL images of ceramics $(0.23ZrO_2–0.77HfO_2)$-Y_2O_3-Eu_2O_3 with various content of yttrium.

shown that yttrium is distributed uniformly in the selected concentration range.

The obtained CL-images are presented in Fig. 1. It can be seen that all samples except for 0.4Eu−9YSZH, have a uniform red luminescence, and the nonuniformity of luminescence is related only to the surface relief. In the sample of 0.4Eu−9YSZH the areas with light luminescence from 40 to 200 μm in size are observed. The CL spectra of all samples contain radiation bands associated with transitions in Eu^{3+} ions, including high-energy transitions($^5D_0$–^7Fj, $^5D_1$–^7Fj and $^5D_2$–^7Fj). The intensity ratios of the bands and their spectral positions are characteristic of hafnium oxide with a cubic crystal structure [16–18]. In CL spectrum of 0.4Eu-9YSZH sample there's an additional band with a radiation maximum of 615 nm. This band is associated with the splitting of transition levels $^5D_0$–$^7F_2$, which occurs in lower-symmetric phases of hafnium oxide, for example, in monoclinic one [18].

According to the method proposed in [16], the asymmetry coefficient was calculated for all samples (Table 2). The decay times were obtained for the most intense transition $^5D_0$–$^7F_1$ (Table 2). It is shown that kinetic curves are well approximated by the sum of two exponentials, which is typical for ceramics:

$$I = I_0 + A_1 \exp\left(-\frac{t}{t_1}\right).$$

We associate the short component of the decay kinetics with the centers located close to the grain boundaries [16,21]. The transition times $^5D_0$–$^7F_1$ in 0.4Eu−9YSZH sample with the lowest yttrium content are noticeably shorter than in the other samples, which indicates a higher content of point defects in this sample. It can be seen that the decay times and their contributions do not depend on the yttrium content at concentrations above 11 mol.%.

It can be seen from the CL spectra that the sample contains 0.4Eu−9YSZH with a yttrium content of 9 mol.% there is a loss of the minor phase and the formation of a large number of point defects: vacancies and poly-vacancies of oxygen. In addition, the appearance of an intense radiation band in the blue range of CL spectrum indicates a high content of point defects in this sample. The high content of point defects is proved by the fact that the decay times in the sample with yttrium content of 9 mol.% are lower than in the rest of the samples in the series. Most likely, the presence of point defects leads to an increase in the probability of non-radiative recombination. For samples 0.6Eu−11YSZH, 0.4Eu−14YSZH and 0.4Eu−16YSZH the decay times do not depend on yttrium content. It is important to note that as the concentration of yttrium rises, the asymmetry coefficient goes up, which is an evidence of a higher amount of less symmetrical centers of europium.

The nature of the contrast in CL image for the sample 0.4Eu−9YSZH was examined in detail (Fig. 2). As can be seen in Fig. 2, regions with different luminescence are observed in the sample. In CL spectrum obtained in the region (1) with bright blue luminescence of sample 0.4Eu−9YSZH, intense wide luminescence bands are ob-

Table 2. Asymmetry coefficients and decay times of transition $^5D_0-^7F_1$

Sample	max $I_{(ED)}/I_{(MD)}$	A_1	τ_1, ms	A_2	τ_2, ms
0.4Eu−9YSZH	0.83	0.47±0.03	0.21±0.05	0.53±0.04	1.2±0.1
0.6Eu−11YSZH	0.94	0.47±0.02	0.31±0.03	0.53±0.02	1.43±0.08
0.4Eu−14YSZH	0.98	0.48±0.11	0.32±0.03	0.52±0.04	1.41±0.05
0.4Eu−16YSZH	1.04	0.49±0.03	0.29±0.02	0.51±0.03	1.29±0.02

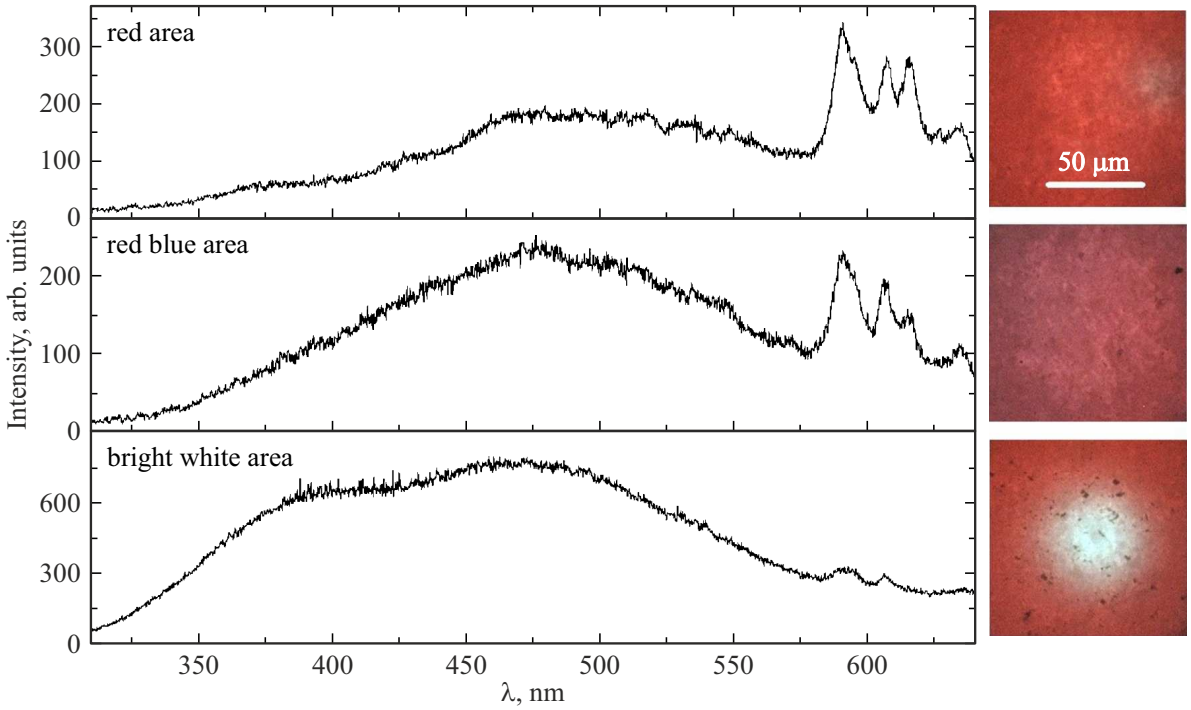

Figure 2. Spectra and CL images of ceramics 0.4Eu-9YSZH.

served in the visible region of the spectrum with radiation maxima of 470 (2.6 eV) and 390 nm (3.2 eV). In region (2), the intensity of both wide bands decrease, while the intensity of the band with a maximum of 3.2 eV is noticeably lower. In the major portion of the sample — a region with a red luminescence band (3) with a maximum radiation of 3.2 eV is actually not observed. In the spectrum, there is mainly a band with a maximum radiation of 2.6 eV, while its intensity becomes even lower. Based on experimental data on the luminescence of these materials, electrophysical studies, photoelectron spectroscopy and quantum chemical modeling, it was found that single oxygen vacancies [22,23] are causing formation of the band with a maximum luminescence of 2.6 eV in HfO_2, ZrO_2, HfZrO. The radiation band decay time 2.6 eV was measured for the sample 0.4Eu−9YSZH. The decay curves are also well approximated by the sum of two exponents with exponents 23±3 μs and 5±1 μs.

The CL intensity dynamics at a wavelength of 500 nm and the absorbed current under steady-state electron beam irradiation were obtained. The wavelength of 500 nm was selected because no luminescence of europium bands is expected at this wavelength, only luminescence associated with point defects. As can be seen from Fig. 3, the CL intensity with time does not depend on Y content and is associated with the growth of a hydrocarbon contamination film in the area of electron beam irradiation directly during irradiation, which effectively absorbs part of the radiation [24].

As can be seen from Fig. 3, the dynamics of the absorbed current clearly depends on the content of Y — the higher the content of Y, the more pronounced the change in the absorbed current. The exponential growth in current during electron beam irradiation is associated with the filling of electron traps during irradiation. This is consistent with the fact that as Y content rises, the number of oxygen vacancies goes up, which act as electron traps in oxide materials [25].

Conclusions

The ceramics $(0.23ZrO_2-0.77HfO_2)$-Y_2O_3-Eu_2O_3 was synthesized containing Y_2O_3 from 9 to 16 mol.%. Analysis

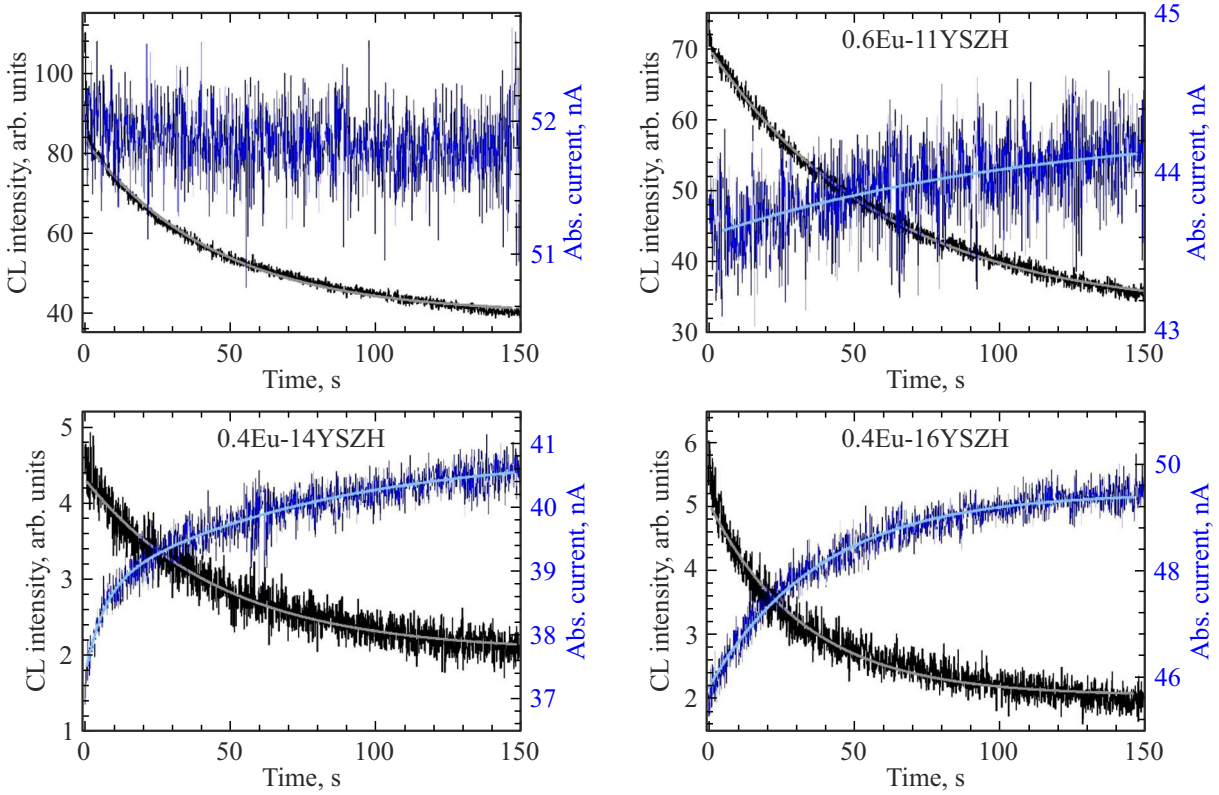

Figure 3. Dynamics of CL-intensity of the 500 nm band (black lines) and dynamics of the absorbed current (blue lines).

of the CL spectra showed that the ceramics are stabilized in the cubic phase. The ceramics containing Y_2O_3 9 mol.% has a monoclinic phase impurity. A clear relationship has been established between the yttrium content and the asymmetry coefficient, which is an evidence of the growing number of Eu^{3+} ions in a lower symmetric position when yttrium content is increased. The study of CL ceramics in the blue and UV ranges revealed an increased number of point defects in a sample containing Y_2O_3 9 mol.%. The studied charge carrier traps demonstrated a regular increase in the number of electron traps with a rise in yttrium concentration.

Funding

The study of the defect bands decay kinetics and traps was supported by grant of the Russian Science Foundation № 24-72-00112, https://rscf.ru/project/24-72-00112/.

Conflict of interest

The authors declare that they have no conflict of interest.

References

[1] D. Nakauchi, G. Okada, T. Yanagida. Scintillation. J. Lumin., **172**, 61 (2016). DOI: 10.1016/j.jlumin.2015.11.028

[2] S. Nikiforov, A. Dauletbekova, M. Gerasimov, Y. Kasatkina, O. Denisova, V. Lisitsyn, M. Golkovski, A. Akylbekova, A.-D. Bazarbek, A. Akilbekov, A. Popov. Crystals, **13** (11), 1585 (2023). DOI: 10.3390/cryst13111585

[3] A. Bagmut, I. Bagmut, V. Zhuchkov, M. Shevchenko. Tech. Phys., **6**, 856 (2012). DOI: 10.1134/S1063784212060035

[4] Q.J. Hong, S.V. Ushakov, D. Kapush, C.J. Benmore, R.J. Weber, A. van de Walle, A. Navrotsky. Sci. Rep., **8** (1), 14962 (2018). DOI: 10.1038/s41598-018-32848-7

[5] Y. Wu, D. Hong, X. Zhong, Y. Niu, X. Zheng. Ceram. Int., **49** (13), 21133 (2023). DOI: 10.1016/j.ceramint.2023.03.280

[6] C. Li, Y. Ma, Z. Xue, Y. Yang, J. Chen, H. Guo. Ceram. Int., **44** (15), 18213 (2018). DOI: 10.1016/j.ceramint.2018.07.030

[7] C. Ren, C. Li, H. Guo, H. Wang, Z. Bai, Y. Ma. Ceram. Int., **48** (11), 16432 (2022). DOI: 10.1016/j.ceramint.2022.02.196

[8] H. Yu, C. Liu, Z. Zhang, S. Huang, Y. Yang, R. Mao, H. Feng, J. Zhao. Chem. Phys. Lett., **738**, 136916 (2020). DOI: 10.1016/j.cplett.2019.136916

[9] E. Montes, P. Ceron, J. Guzmá n−Mendoza, C. Falcony, M. Angel Vallejo, M. Antonio Sosa. Ceram. Int., **44** (7), 8081 (2018). DOI: 10.1016/j.ceramint.2018.01.250

[10] C. Zhao, C. Zhou Zhao, S. Taylor, P.R. Chalker. Materials, **7**, 5117 (2014). DOI: 10.3390/ma7075117

[11] E.J. Shin, S.W. Shin, S.H. Lee, T.I. Lee, M.J. Kim, H.J. Ahn, J.H. Kim, W.S. Hwang, J. Lee, B.J. Cho. IEEE Int. Electron Dev. Meeting (IEDM), 6.2.1 (2020). DOI: 10.1109/IEDM13553.2020.9371984

[12] C. Jin, C. J. Su, Y. J. Lee, P. J. Sung, T. Hiramoto, M. Kobayashi. IEEE T. Electron Dev., **68** (3), 1304 (2021). DOI: 10.1109/TED.2020.3048916

[13] E.V. Dementeva, P.A. Dementev, M.A. Yagovkina, M.V. Zamoryanskaya. ACS Appl. Nano Mater., **6**, 16212 (2023). DOI: 10.1021/acsanm.3c02178
[14] Y. Cao, C. Li, Y. Ma, H. Luo, Y. Yang, H. Guo. Ceram. Int., **45** (3), 12851 (2019). DOI: 10.1016/j.ceramint.2019.03.208
[15] D.R. Belichko, T.E. Konstantinova, A.V. Maletsky, G.K. Volkova, A.S. Doroshkevich, M.V. Lakusta, M. Kulik, A.A. Tatarinova, D. Mardare, C. Mita, N. Cornei. Ceram. Int., **47** (3), 3142 (2021). DOI: 10.1016/j.ceramint.2020.09.151
[16] E.V. Dementeva, A.A. Shakirova, K.N. Orekhova, T.B. Popova, M.A. Yagovkina, A.I. Lihachev, P.A. Dementev, I.D. Venevtsev, A.F. Zatsepin, D.S. Koshelev, V.V. Utochnikova, B. E. Burakov, M.V. Zamoryanskaya. J. Alloys Compd., **1007**, 176452 (2024). DOI: 10.1016/j.jallcom.2024.176452
[17] V.A. Kravets, K.N. Orekhova, M.A. Yagovkina, E.V. Ivanova, M.V. Zamoryanskaya. Opt. Spectrosc., **125**, 188 (2018). DOI: 10.1134/S0030400X18080167
[18] E.V. Ivanova, V.A. Kravets, K.N. Orekhova, G.A. Gusev, T.B. Popova, M.A. Yagovkina, O.G. Bogdanova, B.E. Burakov, M.V. Zamoryanskaya. J. Alloys Compd., **808**, 151778 (2019). DOI: 10.1016/j.jallcom.2019.151778
[19] K. Smits, L. Grigorjeva, D. Millers, A. Sarakovskis, A. Opalinska, J.D. Fidelus, W. Lojkowski. Opt. Mater., **32** (8), 827 (2010). DOI: 10.1016/j.optmat.2010.03.002
[20] A.A. Shakirova, E.V. Dementeva, T.B. Popova, M.V. Zamoryanskaya. Opt. Spectrosc., **131** (3), 172 (2023). DOI: 10.61011/EOS.2023.05.56509.76-22
[21] E.V. Dementeva, A.A. Shakirova, P.A. Dementev, K.N. Orekhova, M.V. Zamoryanskaya. Opt. Spectrosc., **131** (10), 1359 (2023). DOI: 10.61011/OS.2023.10.56887.5619-23
[22] D.R. Islamov, V.A. Gritsenko, V.N. Kruchinin et al. Phys. Solid State, **60**, 2050 (2018). DOI: 10.1134/S1063783418100098.
[23] M.H. Park, C.-C. Chung, T. Schenk, C. Richter, M. Hoffmann, S. Wirth, J.L. Jones, T. Mikolajick, U. Schroeder. Adv. Electron. Mater., **4**, 1700489 (2018). DOI: 10.1002/aelm.201800091
[24] K.N. Orekhova, Y.M. Serov, P.A. Dementév, E.V. Ivanova, V.A. Kravets, V.P. Usacheva, M.V. Zamoryanskaya. Tech. Phys., **64**, 1336 (2019). DOI: 10.21883/JTF.2019.09.48068.43-19
[25] B. Henderson, J.E. Wertz. Adv. Phys., **17** (70), 749 (1968). DOI: 10.1080/00018736800101386

Translated by J.Savelyeva